



University of HUDDERSFIELD

University of Huddersfield Repository

Hourdakis, E., Nassiopoulou, A. G., Parisini, A., Reading, M. A., Van den Berg, Jakob, Sygellou, L., Ladas, S., Petrik, P., Nutsch, A., Wolf, M. and Roeder, G.

Electrical and structural properties of ultrathin SiON films on Si prepared by plasma nitridation

Original Citation

Hourdakis, E., Nassiopoulou, A. G., Parisini, A., Reading, M. A., Van den Berg, Jakob, Sygellou, L., Ladas, S., Petrik, P., Nutsch, A., Wolf, M. and Roeder, G. (2011) Electrical and structural properties of ultrathin SiON films on Si prepared by plasma nitridation. *Journal of Vacuum Science & Technology B: Microelectronics and Nanometer Structures*, 29 (2). 022201. ISSN 1071-1023

This version is available at <http://eprints.hud.ac.uk/id/eprint/12272/>

The University Repository is a digital collection of the research output of the University, available on Open Access. Copyright and Moral Rights for the items on this site are retained by the individual author and/or other copyright owners. Users may access full items free of charge; copies of full text items generally can be reproduced, displayed or performed and given to third parties in any format or medium for personal research or study, educational or not-for-profit purposes without prior permission or charge, provided:

- The authors, title and full bibliographic details is credited in any copy;
- A hyperlink and/or URL is included for the original metadata page; and
- The content is not changed in any way.

For more information, including our policy and submission procedure, please contact the Repository Team at: E.mailbox@hud.ac.uk.

<http://eprints.hud.ac.uk/>

Electrical and structural properties of ultrathin SiON films on Si prepared by plasma nitridation

E. Hourdakis^{a)} and A. G. Nassiopoulou

IMEL/NCSR Demokritos, Terma Patriarchou Grigoriou, Aghia Paraskevi, 153 10 Athens, Greece

A. Parisini

CNR-IMM Sezione di Bologna, Via P. Gobetti 101, 40129 Bologna, Italy

M. A. Reading and J. A. van den Berg

Institute for Materials Research, University of Salford, Salford M5 4WT, United Kingdom

L. Sygellou and S. Ladas

Surface Science Laboratory, Department of Chemical Engineering, University of Patras, Rion, 26504 Achaia, Greece

P. Petrik

Research Institute for Technical Physics and Materials Science, Hungarian Academy of Sciences, H-1121 Budapest, Hungary

A. Nutsch, M. Wolf, and G. Roeder

Fraunhofer Institute Integrated Systems and Device Technology, Schottkystrasse 10, 91058 Erlangen, Germany

(Received 3 September 2010; accepted 31 January 2011; published 2 March 2011)

The authors combined electrical and structural characterizations with analytical and spectroscopic measurements in order to fully analyze oxynitride nanofilms on Si that were produced in a minibatch type plasma nitridation reactor. The authors demonstrate that for the investigated samples the result of nitridation is different in the 2-nm-thick SiO₂ films compared to the 5-nm-thick films. In the first case, nitridation results in an increase of the oxide film thickness compared to the non-nitrided film, with a consequent decrease in leakage current and an increase in the electrically measured equivalent oxide thickness (EOT). In contrast, nitridation of the 5-nm-thick SiO₂ films leads to a reduction of both the leakage current and EOT. Finally, the authors demonstrate that the applied nitridation process results in the desired nitrogen profile with high nitrogen concentration near the top surface or the middle of the SiON film and low nitrogen concentration near the SiON/Si interface, which leads to a relatively low density of interface states at the SiON/Si interface ($\sim 10^{11}$ states/cm²) for nonannealed films. © 2011 American Vacuum Society. [DOI: 10.1116/1.3556938]

I. INTRODUCTION

In the past years aggressive scaling of the gate thickness of SiO₂-based metal-oxide semiconductor field effect transistors (MOSFETs) has led to an increase of the gate leakage current to unacceptable levels. This is due to the fact that direct tunneling leakage current increases exponentially as the dielectric thickness decreases. Since the down scaling of the gate dielectric is essential to the reduction of the MOSFET size, different solutions are investigated as, for example, the replacement of the silicon oxide with oxynitrides or nitrated SiO₂ or high-*k* materials as gate dielectrics.¹

The incorporation of nitrogen in the SiO₂ dielectric serves a number of purposes. One such purpose is to increase the dielectric constant of the material (*k*) allowing for the further reduction of the gate equivalent oxide thickness (EOT). The dielectric constant of the oxynitride depends on the N content. As N is incorporated, *k* increases from the SiO₂ value of

3.9 to a maximum of the Si₃N₄ value of 7.5.² Because of the increase of the dielectric constant, the thickness of the gate material can be increased without loss of the EOT.³ Therefore, the gate leakage current can be lowered and a reduction of at least one order of magnitude compared to the equivalent SiO₂ dielectric is usually observed.⁴⁻⁶ Finally, nitrogen forms a barrier against the diffusion of dopants, especially boron atoms, from the highly doped polysilicon gate to the dielectric.^{2,4-7} This diffusion has detrimental effects to the reliability of the dielectric material.² Therefore, nitrogen incorporation increases the thermal stability of the gate dielectric.

Despite the many advantages of the use of oxynitrides as gate material, the introduction of N in the SiO₂ has certain disadvantages. There is a decrease of the oxide band gap energy with increasing N incorporation which results in a lower barrier for direct tunneling.^{2,5} As a consequence an increased gate leakage current is expected in this case compared to non-nitridated SiO₂ of the same physical thickness. This means that a physically thicker oxynitride film is re-

^{a)}Electronic mail: mhour@imel.demokritos.gr

quired at high nitrogen concentration in order to obtain the same electrical EOT value for overall leakage current reduction.^{2,3,6}

Additionally, an enhanced defect density has been observed in the case of N pileup at the Si/SiO₂ interface.^{4,6,8} The value of the density of interface states (D_{it}) for thin oxynitride films typically increases with nitrogen concentration.⁶ A typical value of D_{it} for oxynitrides without postnitridation annealing and for a N concentration of around 5% is $D_{it} \sim 10^{11} \text{ cm}^{-2}$,^{6,9,10} while values as high as 10^{13} cm^{-2} were also measured.¹¹ Further annealing at high temperatures can passivate the surface and help reduce the value of D_{it} .¹¹ Values as low as $\sim 10^{10} \text{ cm}^{-2}$ have been achieved using such annealing procedures.¹² The increase in D_{it} following nitridation can degrade the channel mobility. It can also cause reliability issues such as a deterioration of the negative bias temperature instability.^{3,9,13,14} This phenomenon is one of the major reliability issues faced by ultrathin gate dielectrics. It is therefore important to control the vertical distribution of N in the oxynitride film, especially for very thin films. An optimum distribution would be a high N concentration close to the poly-Si/oxynitride interface that leads to a reduction in dopant penetration and an increase in the k value and a low N concentration at the Si/oxynitride interface that leads to reduction of the interface states and therefore increased channel mobility.

There are several methods for creating oxynitrides. The most popular ones are thermal nitridation and annealing of SiO₂ in NO or N₂O.² These two methods require high temperatures and generally result in a low N concentration in the final oxide [from a monolayer to $\sim 5\%$ (Refs. 2 and 13)]. Nitridation in NH₃ results in the incorporation of larger amounts of N [$\sim 10\% - 15\%$ (Refs. 2 and 12)] but it suffers from the fact that the N piles up at both interfaces. Additionally, it introduces a high concentration of H in the films, which further increases the density of states at the Si/dielectric interface.² Plasma nitridation methods, on the other hand, have attracted attention recently because they can produce the desired N profile. The temperatures involved are typically lower than those of the thermal processes. They can be tuned to allow for higher N concentrations near the oxynitride/poly-Si interface and a low N concentration near the Si/oxynitride interface while maintaining an overall large N incorporation (N concentrations from 2% to $\sim 50\%$ are possible^{3,5-7,9,11,13}). This control over the N depth profile makes plasma nitridation the best choice for ultrathin (<3 nm) oxides.

Ultrathin oxynitrides have also been used recently as interfacial layers in a stack of high- k materials¹⁵ with small total EOT. Commercially available high- k (Hf-based) gate dielectric MOSFETs are already in production since a few years.¹⁶ Commonly used high- k materials, though, have very poor thermodynamic stability on Si and surface engineering is required for their stabilization, the most commonly used being the fabrication of an ultrathin SiO₂ interfacial layer on the Si substrate between Si and the high- k material. The existence of this low- k interfacial layer limits the reduction of

TABLE I. SiON samples and corresponding process parameters.

Wafer ID	03	05	07	33
SiO ₂ thickness (nm)	2	2	2	5
Nitridation process time	60 min	10 min	Off	60 min

the EOT since the capacitance of the high- k /SiO₂ stack depends ultimately on the SiO₂ capacitance. For further scaling down of the above dielectric stack thickness, nitridation of the SiO₂ interfacial layer is performed in order to increase its k value.^{17,18}

With the present widespread use of ultrathin oxynitrides as gate dielectrics by the industry, it is important that a batch wafer process is used for SiO₂ nitridation. Plasma techniques described above as the most suitable for high level N incorporation have been demonstrated in most cases^{6,7} in laboratory equipment not necessarily suited for mass production. In the following, we examine the nitridation of thin SiO₂ films produced in a minibatch reactor, capable of processing simultaneously various wafer size samples, which is therefore closer to industrial needs. The purpose of this work is to present a careful analysis of the samples produced in this manner by applying electrical, structural, compositional (depth profiles), and optical measurements and correlate the results obtained by the different methods in order to facilitate a better understanding of the capabilities of the method.

II. EXPERIMENT

A. Sample fabrication

The thin oxynitride films used in this work were fabricated by plasma nitridation of thin SiO₂ films on Si using a prototype minibatch furnace that employs a combination of direct pulsed low-frequency plasma and remote microwave plasma. The substrates used were p -type (100)-oriented silicon wafers of 150 mm diameter with a specific resistivity of 4–6 $\Omega \text{ cm}$. The wafers were cleaned and subsequently oxidized using dry oxidation. Four different samples were used, as shown in Table I. The thicknesses of the produced SiO₂ film were 2 nm in the case of samples 03, 05, and 07 and 5 nm in the case of sample 33. Nitridation was performed using a N₂/NH₃ feed gas mixture plasma. The direct plasma was generated above the wafers in the spacing of stacked electrodes. Process time was 10 min for sample 05 and 1 h for samples 03 and 33. Sample 07 is a reference sample. Table I gives an overview of the samples used.

B. Characterization techniques

Electrical measurements were performed on MOS devices with Al metallization. The area of the capacitors was $200 \times 200 \mu\text{m}^2$. Ohmic contacts were fabricated on the backside of the wafers to reduce series resistance effects. For simplicity of fabrication, Al metallization was used as gate metal instead of the poly-Si gate used in the industry or more exotic metals usually used in combination with high- k dielectrics. The use of Al might introduce a slightly larger leakage

current but does not greatly affect the measured quantities. As will be shown later the electrical results acquired using an Al gate are qualitatively and quantitatively consistent with the structural and compositional analysis and therefore provide accurate enough information for the investigated quantities.

X-ray photoelectron spectroscopy (XPS) was performed with nonmonochromatic Mg $K\alpha$ radiation, constant 100 eV pass energy on the EA200 analyzer, and an analyzed area of 4×7 mm². The analyzed depth is practically 0–10 nm. The analysis took place along the surface normal (0°) and also at a specimen tilt angle of 45° , as well as at random azimuth in order to average out at least a part of substrate crystallinity effects. For spectra collection and treatment (including peak fitting), the commercial software SPECSLAB1 (by Specs) was used. The practical attenuation lengths were taken as 90% of the corresponding inelastic mean-free-path (IMFP), λ , as obtained according to ISO18118:2004(E). The average relative atomic composition of the films was obtained via the average-matrix-relative-sensitivity-factor-like empirical relative sensitivity factor collection of Wagner, adapted to the EA200 analyzer transmission characteristics and including an average surface “carbon” contamination of 0.8 ± 0.1 nm. In order to calculate IMFP and the parameters necessary for individual layer thickness estimation, material properties of nitrated layers as a function of N content were employed.¹⁹ In all cases, the spectrometer was properly calibrated both with respect to the energy scale and the intensity scale, according to relevant International Standards.

Spectroscopic ellipsometry (SE) measurements were performed by a Woollam M-2000DI rotating compensator ellipsometer in the wavelength range of 190–1700 nm at angles of incidence of 65° , 70° , and 75° . One-layer and two-layer optical models were used for the evaluation. The one-layer model consisted of a Si substrate and a Cauchy overlayer that describes the dispersion of the refractive index using $n = An + Bn/\hat{\lambda}^2 + Cn/\hat{\lambda}^4$, where n is the refractive index, λ denotes the wavelength of light in nanometers, and An , Bn , and Cn are the Cauchy parameters. The two-layer model assumed an interface layer between the Cauchy layer and the substrate. This interface layer is a 50%–50% “mixture” of substrate and layer material calculated by the Bruggeman effective medium theory.

Transmission electron microscopy (TEM) measurements were performed using a F.E.I. Tecnai F20 ST TEM/scanning transmission electron microscopy (STEM) operating at 200 kV. High resolution electron microscopy (HREM) and Z-contrast high angle annular dark field (HAADF)-STEM imaging were used.

Medium energy ion scattering (MEIS) analysis was carried out using the following scattering conditions: 100 keV He⁺ ions, incident along the $[\bar{1}\bar{1}1]$ channeling direction and detected along both the $[111]$ and $[332]$ blocking directions. The effective near-surface depth resolution for these conditions is 0.8 nm, which is determined from the slope of the leading edge of the Si peak recorded on a clean Si surface and is caused by a combination of the energy resolution of

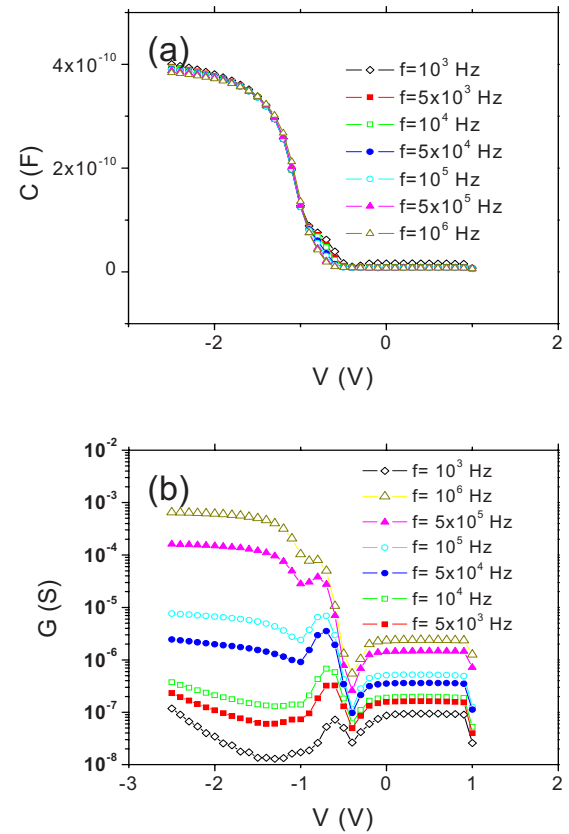


FIG. 1. (Color online) Capacitance (C)-voltage (V) measurements (a) and conductance (G)-voltage (V) measurements (b) in the high frequency region for sample 03 (2 nm nominal thickness and 60 min plasma nitridation).

the system combined with straggling. The deconvolution of the energy spectra into depth profiles of multilayers containing different masses is a complex task. To make this process as accurate and efficient as possible a simulation program was used based on the IGOR© graphing package.²⁰

III. RESULTS AND DISCUSSION

In the following we present the results of the electrical, XPS, TEM, and MEIS characterizations and ellipsometric measurements separately as each technique yields results independent of the other ones. In Sec. IV we correlate the different results and demonstrate that the information acquired by each method separately can be combined to produce a good understanding of the SiON samples' properties.

A. Electrical characterization

Capacitance (C)-voltage (V) and conductance (G)-voltage (V) measurements for different frequencies were performed on all devices. Typical results of such measurements for sample 03 are presented in Fig. 1. The slight frequency dispersion of the C - V curves in accumulation can be attributed to a series resistance effect. This is evident from the fact that the value of capacitance in accumulation decreases with increasing frequency. The frequency dispersion of the curves around $V_G = -0.6$ V is characteristic of the existence of interface traps.

TABLE II. Results of electrical characterization for all samples. Series resistance (R_s), oxide capacitance (C_{ox}), EOT, and density of interface states (D_{it}) are presented.

Sample	03	05	07	33
R_s (Ω)	104	110	...	182
C_{ox} (F)	4.17×10^{-1}	5.3×10^{-10}	6.1×10^{-10}	3.3×10^{-10}
EOT (nm)	3.4	2.6	2.3	4.3
D_{it} (states/cm ²)	$5.65 \cdot 10^{11}$	$6.24 \cdot 10^{11}$...	$6.04 \cdot 10^{11}$

We have used the capacitance and conductance measurements to estimate the value of the series resistance for each sample through the relation^{21,22}

$$R_s = \frac{G_{acc}}{G_{acc}^2 + \omega^2 C_{acc}^2}, \quad (1)$$

where R_s is the series resistance, G_{acc} is the conductance of the sample at accumulation, C_{acc} is the capacitance of the sample at accumulation, and ω is the measurement frequency. The value of R_s is used as a correction factor in the determination of the density of interface states discussed later.

We have also used the Maserjian method for determining the oxide capacitance, C_{ox} , for our samples.²² We have then used the following relation to determine the oxide thickness t_{ox} or the oxide permittivity ϵ_{ox} :

$$t_{ox} = \frac{\epsilon_{ox} \epsilon_0 A}{C_{ox}}, \quad (2)$$

where ϵ_0 is the vacuum permittivity and A is the capacitor area. We have calculated the value of the EOT based on Eq. (2) and using C_{ox} deduced from the C - V curves and $\epsilon_{ox} = \epsilon_{SiO_2} = 3.9$. The results for all the above measured values are presented in Table II (from this point forth we will use the word thickness to mean physical thickness, while we will use the acronym EOT to refer to the electrically measured equivalent oxide thickness). The EOT values reveal an interesting trend for the samples. Sample 07 has an EOT value very close to the nominal thickness value of 2 nm. This implies that the nitridation process without plasma has very little or no effect on the SiO₂ film. In contrast, the EOT values of samples 05 and 03 are larger than the nominal thickness. Moreover, the EOT value of sample 03 (plasma for 60 min) is larger than the one of sample 05 (plasma for 10 min). This suggests that the process time of plasma nitridation increases the thickness of the initial SiO₂ film. This observation has been previously reported⁵ on similar samples for different nitridation techniques.

In order to determine the density of the interface states (D_{it}) present in the samples, their conductance ($G_p(\omega)$) was measured as a function of frequency. An example of such a measurement for sample 03 is given in Fig. 2. The conductance method is then used to extract the value of D_{it} .^{21,23} The results of this determination are presented in Table II. These values are on the order of 10^{11} states/cm² for all samples. This value is rather low for nitrated SiO₂ films that have

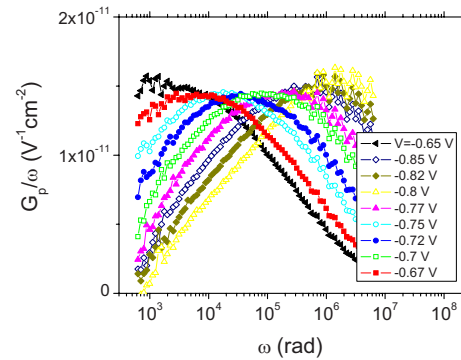


FIG. 2. (Color online) Experimental trap conductance G_p over frequency ω vs ω curves for sample 03 (2 nm nominal thickness and 60 min plasma nitridation).

undergone no annealing. Similar values have been observed in samples with a nitrogen concentration of about 5%, as was discussed in Sec. I.^{6,9,10} The determination of the value of D_{it} for sample 07 was impossible due to large leakage currents.

Finally, current (I)-voltage (V) curves have been measured for all samples. The results appear in Fig. 3. Clearly, sample 33 has the smallest leakage current, as expected due to its higher nominal thickness of 5 nm. For the samples of nominal thickness of 2 nm, it can be seen that the highest leakage current is measured in sample 07 and the lowest in sample 03. We have to note that there is a shift in the point of polarity change of the measured current (the minimum of the current on the semilogarithmic plot) for the samples with the lowest values of current or the longest processing times. This is reasonable as the value of the leakage current in these samples is very small, especially in the case of samples 03 and 33 and is therefore close to the detection limit of the instrument used. So any change in the interface states of the SiON layer with Si will result in a shift of that minimum. This shift should be more pronounced for the smaller leakage current measurements. It is also reasonable to expect that the nitridation process introduces fixed charges, so the charging is more pronounced in the case of longer processing times.

The above results are consistent with the apparent increase in film thickness with plasma nitridation duration, as suggested by the EOT results of Table II. As the thickness of

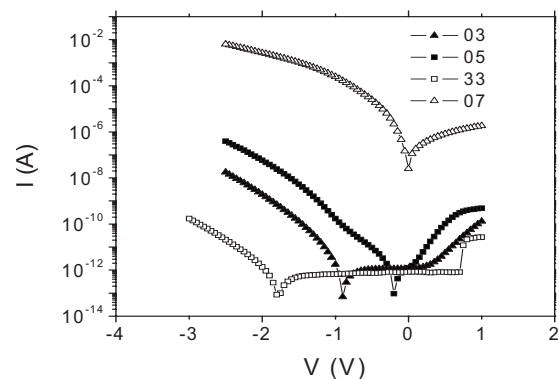


FIG. 3. Leakage current (I)-voltage (V) characteristics for all samples.

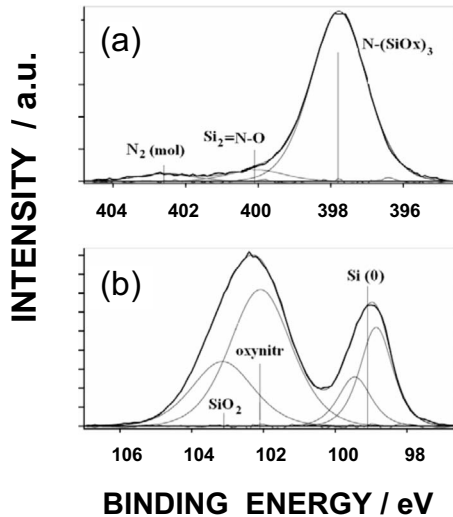


FIG. 4. (a) XPS spectra from the N $1s$ region in sample 03 (2 nm nominal thickness and 60 min plasma nitridation) fitted with three components due to differently bonded N inside the oxynitride layer. (b) XPS spectra from the Si $2p$ region in sample 03 (2 nm nominal thickness and 60 min plasma nitridation) fitted with two narrow components for the $2p$ doublet for Si(0), as well as single broad components for the $2p$ doublet from a N-rich environment and a nearly N-free environment in the oxynitride layer.

the dielectric increases, the value of the leakage current is reduced. Had the nitridation process left the film thicknesses unaffected, the results would be opposite. As was discussed in Sec. I, the addition of nitrogen reduces the barrier for direct tunneling through the SiO_2 films. Therefore, the longer the oxidation time, the larger the leakage current should be expected.

B. Structural characterization

1. XPS

The increase in oxide capacitance and EOT values apparent in the electrical measurements only in the case of the 2-nm-thick samples necessitated the further analysis using a technique that can provide information on both the sample thickness and the average nitrogen content or equivalently the value of the dielectric constant. To that end XPS measurements were employed, which yield directly the chemical state and an average atomic content over the analyzed depth. In addition, by measuring at two different tilt angles, qualitative indication of any significant nonuniformity in the in-depth distribution can be obtained. The results are complementary and consistent with the MEIS measurements, which yield an accurate in-depth distribution but need to be integrated over depth to provide the overall atomic composition.

The examples of fitted spectra of the Si $2p$ and N $1s$ regions are shown in Figs. 4(a) and 4(b) for sample 03 analyzed along the surface normal. The Si $2p$ region was fitted with two narrow [1.1 eV full width at half maximum (FWHM)] peaks for the $2p_{1/2}$ and $2p_{3/2}$ components around 99 eV binding energy (BE) from substrate elemental silicon and two broader (2.1 eV FWHM) peaks at ~ 103.2 and ~ 102 eV BEs, each one, respectively, assigned to the combined $2p$ doublet from nearly nitrogen-free (SiO_x) and nitrogen-rich (SiO_xN_y) environments within the oxynitride layer. The N $1s$ region is fitted with three peaks (1.9 eV FWHM) at 397.8, 400.5, and 402.6 eV BEs, of which the first ($\sim 90\%$ of the total peak area) is due to N bonded mainly to Si, the second ($\sim 6\%$ of the area) is due to $\text{Si}_2=\text{N}-\text{O}$ like species, and the third arises from interstitial molecular N_2 which is known to be present in small amounts in nonannealed oxynitrides prepared by plasma nitridation.²⁴

The peak areas from spectra such as shown in Fig. 4 as well as from O $1s$ spectra can be used for the simultaneous estimation of the total average atomic nitrogen content, $100^* \text{N}/(\text{N}+\text{O}+\text{Si}_{ox})$, as well as of the oxynitride layer thickness.¹⁹ These results and an estimate of the dielectric constant for all samples are presented in Table III. The two different values for each quantity correspond to the 0° and 45° XPS measurements, respectively. The estimate for the dielectric constant was made by considering that the dielectric constant changes linearly with nitrogen concentration from the value of 3.9 in the case of SiO_2 (0% N concentration) to 7.5 in the case of Si_3N_4 (100% N concentration).² The fact that the obtained oxynitride thickness values for the two exit angles are not very different indicates that the interfaces are relatively sharp. Furthermore, the fact that the N content does not vary significantly with angle suggests that the expected nonuniformity with depth is not very large and in any case it is larger in the thin nitrided layers, the N content increasing away from the top surface of the oxynitride layer. The latter conclusion is consistent with the presence of a thin, almost N-free, SiO_x region in the oxynitride layer as suggested in Fig. 4(a) for sample 03.

It can be seen from the results of Table III that the reference sample 07 has a thickness of 2.3 nm and contains no nitrogen at all. We observe that the thickness and average nitrogen content of the nominally 2-nm-thick samples are increased with the duration of plasma nitridation. This is evident from the results of samples 05 (10 min of plasma) and 03 (60 min of plasma). Finally, the nominally 5-nm-thick sample 33 has a large amount of nitrogen incorporated (16%) without any increase to its thickness.

TABLE III. XPS results of film thickness, N content, and dielectric constant estimate for all samples.

Sample	03	05	07	33
Thickness (nm) (0° – 45°) (± 0.1 nm)	3.8–4.1	3–3.2	2.3–2.5	5–5.1
N content (0° – 45°) ($\pm 2\%$)	25%–22%	16%–14%	0%–0%	16%–16%
Dielectric constant (ϵ) (0° – 45°)	4.8–4.7	4.5–4.4	3.9–3.9	4.5–4.5

TABLE IV. SE results of film thickness, refractive index, and interface thickness for all samples.

Sample	03	05	07	33
Thickness (nm)	4.2	3.4	2.3	5.1
Refractive index, n	1.83	1.81	1.87	1.75
Interface thickness (nm)	0.6	0.7	0.1	0.3

2. SE

We have also employed spectroscopic ellipsometry measurements as a means of determining the samples' thicknesses by a reference free method. The results are presented in Table IV. It can be seen that the layer thicknesses determined by SE are in a good agreement with those measured by XPS (Table III), confirming that the layer thickness increases with nitridation time. The refractive index also increases with nitridation time, although the refractive index of sample 07 (reference) is higher than that of samples 05 and 03. The reason is that for very thin layers the interface effect becomes significant, increasing the effective refractive index. This is also supported by the fact that sample 33, the thickest sample at nominally 5 nm, has the lowest refractive index. For samples 03 and 05 the refractive index correlates with the nitrogen content. However, this behavior can only be compared for similar layer thicknesses because of the interface effect mentioned above. It is also important to note that the thickness of the interface layer increases with nitridation. The increase is larger for the thinner layers (samples 03 and 05) than for the thicker ones (sample 33).

3. TEM/STEM

The thickness values of samples 03 and 05 obtained by the XPS and SE measurements are much larger than their nominal value of 2 nm. Since in both cases the thickness is deduced indirectly from the experimental result, a more direct measurement of film thickness of sample 05 using TEM/STEM measurements was performed. To this end, HREM and HAADF-STEM techniques were employed. The interest of using both of these microscopy techniques lies in the possibility to compare a "structural" (HREM) and a "compositional" thickness (Z-contrast). Although a detailed report on this comparison will be reported elsewhere, we mention that on sample 05 these different thickness determinations were found in good agreement. The agreement with an incoherent technique such as HAADF-STEM also confirms that HREM phase contrast artifacts were effectively minimized. At the basis of this result is the assessment of a protocol to maximize the amplitude contrast in HREM images and to obtain a value for the film thickness reliably. An example of the starting step of this procedure is shown in the HREM micrographs reported in Fig. 5. Typically, in an electron microscope with uncorrected spherical aberration, HREM intensity modulation mechanism, due to the active phase contrast, may hinder the visibility of an interface or, in presence of crystalline regions, introduce errors in its location (delocalization effects). These effects are both dependent on the mi-

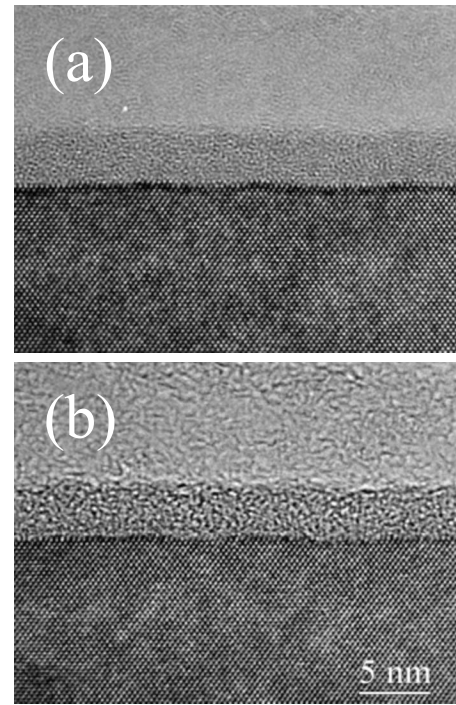


FIG. 5. Cross-sectional HREM micrographs of the nominally 2-nm-thick oxide sample 05 taken on the same region at two different defocus values: (a) minimum contrast condition; (b) optimum defocus condition.

croscopy defocus settings used. The HREM micrographs reported in Figs. 5(a) and 5(b) have been taken on the same sample area at two different defocus values, the so-called minimum and optimum contrast conditions, respectively. A comparison of the two micrographs shows that in Fig. 5(a), the SiON layer is nicely separated from adjacent layers and delocalization effects are minimized. From this micrograph, following a procedure already used in both coherent and incoherent observations, surface and interface positions were determined by locating the inflection points of averaged line profiles taken in a direction normal to the sample surface.²⁵ Repeating this procedure in different areas of the sample resulted in an average layer thickness of 3.6 ± 0.2 nm. Within the limit of the experimental uncertainty, this value is in agreement with those obtained on the same sample by XPS and SE and in any case much higher than the nominal value of 2 nm.

4. MEIS

Besides the increase in EOT in the case of the 2-nm-thick samples with nitridation, the electrical characterization also revealed a relatively low density of interface states for these nonannealed samples. As mentioned in Sec. I, the interface states are related to the nitrogen depth profile or the nitrogen pileup at the interface between the SiON and the Si substrate. In order to acquire the nitrogen depth profile MEIS analysis was employed.

The energy spectra recorded at a scattering angle of 70.5° for the four samples investigated are presented in Fig. 6. The changes in the scattering peaks for Si, O, and N in compari-

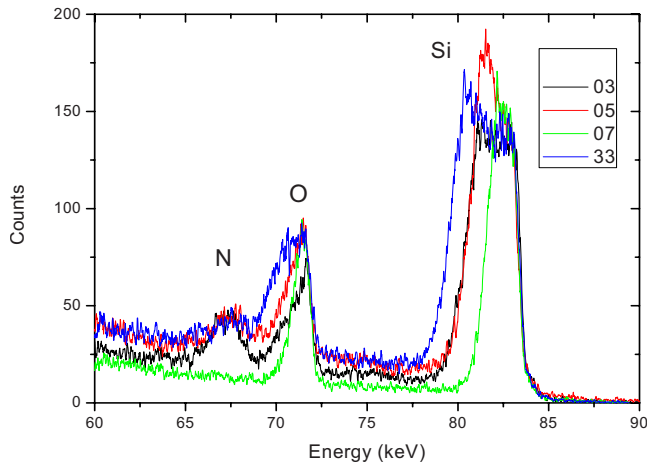


FIG. 6. (Color online) MEIS spectra for all samples using 100 keV He ions incident along the $[\bar{1}\bar{1}1]$ direction and detected along the $[111]$ direction.

son with the reference sample 07 are clearly visible. These energy spectra were modeled using the IGOR© based simulation program to extract the depth profiles for each element observed in the spectra. The depth profile results are split into two groups, i.e., 2 nm and 5 nm, for easy comparison. Figure 7 shows the effect of plasma nitridation including the effect of increasing the plasma exposure from 10 to 60 min for the case of the 2 nm SiO₂ samples.

MEIS indicates that sample 07 (reference) has an oxide layer of 1.4 nm thickness as determined by the half height of the downslope of the O profile. The oxide is confirmed to be stoichiometric at the surface: $\sim 67\%$ O and $\sim 35\%$ Si. After 10 min plasma nitridation (sample 05), the first thing to note is that the N level in the samples is between 15% and 20% to a depth of 3–4 nm, which is clearly deeper than the original oxide of nominally 2 nm and consistent with the XPS analysis. This N concentration is increased in the case of the 60

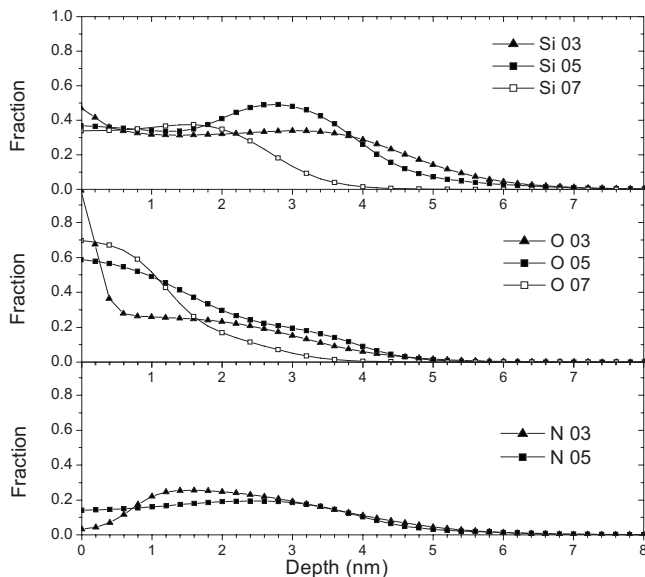


FIG. 7. Si, O, and N depth profiles for samples 03, 05, and 07 (all of 2 nm nominal thickness).

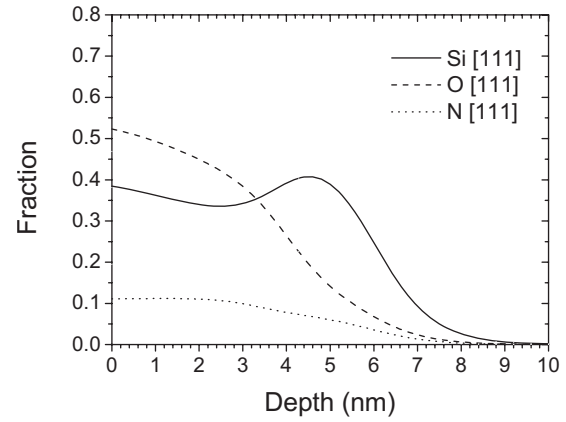


FIG. 8. Si, O, and N depth profiles for sample 33 (5 nm nominal thickness).

min exposure sample (sample 03) below a depth of 1 nm. Second, both the Si disorder and O depth profiles after this process extend to a greater depth into the sample. Interestingly, it appears that the O profiles extend to a similar depth as the N ones, suggesting that the N plasma treatment causes the relocation of O deeper into the sample through collisional or assisted O migration processes. The N profile suggests that the majority of the N concentration is near the upper interface and the center of the created SiON film and is reduced toward the Si/SiON interface. Another observation regarding these profiles refers to what occurs within the first 0.5 nm of the surface after the 60 min plasma exposure (sample 03). A small rise in the Si and a substantial increase in the O fraction are seen along with a corresponding drop in the N profile which is ascribed to postprocess near-surface reoxidation. Although the increase of the O fraction for sample 03 is real as shown by the energy spectrum in Fig. 6, the size of the very large sharp increase in the O profile in Fig. 7 is not realistic and can be ascribed to an artifact of the normalization in the simulation caused by the very narrow width (<0.4 nm) of this layer.

The same analysis was performed on the nominally 5-nm-thick SiO₂ sample 33 processed for 60 min. The results are shown in Fig. 8. As in the nominally 2 nm surface oxide samples, the N is seen to penetrate to the same depth as the O, followed by an increase in Si disorder just below the oxide layer, as expected. From the N profile, a N concentration of $\sim 12\%$ can be deduced, a result consistent with XPS. As in the case of the previous samples, N is distributed mainly toward the upper surface and the middle of the oxynitride film, while it drops to levels below 5% toward the Si/SiON interface.

IV. DISCUSSION

Considering first the reference sample 07, as expected neither XPS nor MEIS shows it to contain any traces of N. Although MEIS suggests a thickness of 1.4 nm, XPS suggests 2.4 nm. These results are consistent with the observation that from the electrical measurements the EOT of sample 07 is very close to the nominal thickness of the SiO₂ film.

TABLE V. Comparison between the electrical and XPS results for each film's EOT.

Sample	03	05	07	33
EOT (electrical) (nm)	3.4	2.6	2.3	4.3
EOT (XPS) (nm) (00–450)	3.1–3.4	2.6–2.8	2.3–2.5	4.3–4.4

Upon plasma nitridation there is N incorporation and the creation of SiON films. The amount of nitrogen incorporated depends on the duration of exposure to the plasma by both the XPS and MEIS measurements in the case of the nominally 2-nm-thick films (samples 05 and 03). The amounts of nitrogen added have been shown to be 16% and 25% in the case of 10 and 60 min exposures, respectively. The plasma nitridation process is thus more effective than chemical methods and comparable to other plasma methods in nitriding thin films, as discussed in Sec. I. In the case of the 5-nm-thick sample 33, the total amount of nitrogen has been shown to be 16%, even though the exposure duration was 60 min. This, of course, is a result of the film larger thickness. The same amount of N added to a film will result in a different percentage of the final film according to the film thickness.

Second, it is seen from the measurements that there is an increase in the thickness of the original 2-nm-thick SiO₂ film upon nitridation. This has been demonstrated quantitatively through XPS and SE measurements, confirmed by direct TEM/STEM observations, and also qualitatively shown through the MEIS characterization. This increase in the film thickness is also readily demonstrated by the increase in the films' EOT, shown by the electrical measurements, despite the introduction of nitrogen and, hence, the increase of the films' dielectric constants. A direct comparison between the results of the electrical and structural characterizations is possible if we compare the EOT of each sample attained through the electrical measurements and an EOT calculated for each film using the XPS results. As shown above, the XPS results include the thickness of the SiON films but also the N concentration and therefore the value of the dielectric constant. We can calculate the EOT for each film using

$$\text{EOT} = d_{\text{measured}} \frac{\epsilon_{\text{SiO}_2}}{\epsilon_{\text{estimated}}}, \quad (3)$$

where d_{measured} is the measured thickness, $\epsilon_{\text{SiO}_2}=3.9$ is the value of the dielectric constant for SiO₂, and $\epsilon_{\text{estimated}}$ is the estimated value of the dielectric constant. The results for both the electrical measurement EOT and the XPS EOT are given in Table V. The agreement between the results is extremely good.

In the case of the 5-nm-thick film (sample 33) there is no increase in film thickness observed due to nitridation. In this case, the addition of nitrogen increases the value of the dielectric constant of the material. Therefore, we would have expected the behavior observed, i.e., a decrease of the film EOT from 5 to 4.3 nm.

A possible explanation for the observed increase of the 2 nm nominal thickness films with nitridation time can be explained by reoxidation caused by N radicals.^{5,26} High energy nitrogen radicals interact with Si atoms near the Si/SiO₂ interface releasing oxygen atoms. These atoms then diffuse into the Si substrate causing reoxidation and hence an increase in the physical thickness of the dielectric. The increase in physical thickness is accompanied by an increase in dielectric constant due to the introduction of nitrogen with the former being the dominant effect which leads to an increase of the EOT. In the case of the 5-nm-thick film this mechanism is absent since the N radicals do not seem to be energetic enough to reach the Si/SiO₂ interface and break up the SiO₂ bonds. So there is no increase of the physical thickness, only an increase of the dielectric constant and so a decrease of the EOT is observed.

The increase in film thickness demonstrated above quantitatively can also explain the decrease of leakage current with nitridation in the case of the 2-nm-thick samples. As discussed, the introduction of nitrogen in the films should lead to an increase in leakage current since there is a lowering of the potential barrier for tunneling. The increase in film thickness, though, should result in a decrease of the leakage current. The latter effect prevails in the behavior of the material in the case of the leakage current, as in the case of the EOT behavior.

The final conclusion that can be drawn from our measurements concerns the depth profile of the nitrogen. MEIS characterization showed that the nitrogen extends to the same depth as oxygen in the nitrated samples. It also shows that the majority of the incorporated nitrogen is located near the upper surface or the middle of the SiON film and becomes reduced near the Si/SiON interface. As can be seen in Fig. 7 there is appreciable extend over that interface. This fact is quite common for oxynitrides.^{6,10} The important feature is that the nitrogen concentration does not peak near the Si/SiON interface as in previous examples in the literature^{6,10} but rather is distributed along the entire depth of the oxynitride. Nitrogen pileup near that interface causes a large number of interface states. Our electrical results show that the value of the density of interface states (D_{it}) for all our samples is on the order of 10¹¹ states/cm². This value is typical for samples that have not undergone any annealing process but have a much lower N concentration (~5%) than our samples, as was explained in Sec. I. Hence, the value of D_{it} correlates very well with the reduction of the nitrogen percentage near the Si/SiON interface.

V. CONCLUSIONS

In this paper the successful nitridation of SiO₂ thin films using a plasma technique was demonstrated by applying complementary characterization techniques as electrical measurements, TEM, MEIS, XPS, and spectroscopic ellipsometry. Furthermore, it was pointed out that the plasma nitridation process increases the thickness of SiO₂ films of initially 2 nm thickness. The increase is related to the time of the nitridation and it results in an increase of the films' EOT.

Electrical analysis demonstrated that the nitridation significantly reduces the leakage current through the films. In the case of the 5-nm-thick SiO₂ sample, the nitridation process does not affect the thickness of the film. The addition of nitrogen is therefore effective in reducing the film's EOT.

We have demonstrated that the nitrogen profile in the resulting SiON films is very close to the desired one. The majority of the nitrogen is concentrated either on the metal/SiON interface or in the center of the SiON film and this results in a relatively small density of interface states ($D_{it} \sim 10^{11}$ states/cm²) for the examined films that were not annealed.

ACKNOWLEDGMENTS

This work was partially funded by the European Commission in FP6 "ANNA" project, Contract Nos. 026134_RII3, SEA-NET, IST-027982. The authors would also like to acknowledge W. Lerch and M. Rambach for sample preparation.

¹R. M. Ramanathan and R. Willoner, Intel white paper, http://download.intel.com/technology/silicon/silicon_paper_06.pdf.

²M. L. Green, E. P. Gusev, R. Degraeve, and E. L. Garfunkel, *J. Appl. Phys.* **90**, 2057 (2001).

³V. D. Maheta, C. Olsen, K. Ahmed, and S. Mahapatra, *IEEE Trans. Electron Devices* **55**, 1630 (2008).

⁴S. Y. Tan, *Microelectron. J.* **38**, 783 (2007).

⁵C.-H. Chen *et al.*, *IEEE Trans. Electron Devices* **49**, 840 (2002).

⁶K. Watanabe, T. Tatsumi, M. Togo, and T. Mogami, *J. Appl. Phys.* **90**, 4701 (2001).

⁷S. Murakawa *et al.*, *Jpn. J. Appl. Phys.* **47**, 5380 (2008).

⁸C.-Y. Hu, S.-C. Chen, J. F. Chen, S.-J. Chang, M.-H. Wang, V. Yeh, and J.-C. Chen, *J. Vac. Sci. Technol. B* **25**, 1298 (2007).

⁹S. U. Han, H. S. Kang, and B. K. Kang, *Microelectron. Eng.* **83**, 520 (2006).

¹⁰D. Bouvet, P. A. Clivaz, M. Dutoit, C. Coluzza, J. Almeida, G. Margariton, and F. Pio, *J. Appl. Phys.* **79**, 7114 (1996).

¹¹R. Perera, A. Ikeda, R. Hattori, and Y. Kuroki, *Thin Solid Films* **423**, 212 (2003).

¹²C. H. Lai, B. C. Lin, K. M. Chang, K. Y. Hsieh, and Y. L. Lai, *Jpn. J. Appl. Phys., Part 1* **45**, 4898 (2006).

¹³Y. Mitani, H. Satake, and A. Toriumi, *IEEE Trans. Device Mater. Reliab.* **8**, 6 (2008).

¹⁴J. Yang *et al.*, *Appl. Phys. Lett.* **94**, 082103 (2009).

¹⁵G. D. Wilk, R. M. Wallace, and J. M. Anthony, *J. Appl. Phys.* **89**, 5243 (2001).

¹⁶K. Mistry *et al.*, *Tech. Dig. - Int. Electron Devices Meet.* **2007**, 247.

¹⁷D. Ishikawa, S. Kamiyama, E. Kurosawa, T. Aoyama, and Y. Nara, *Jpn. J. Appl. Phys.* **48**, 04C004 (2009).

¹⁸V. Edon *et al.*, *J. Electrochem. Soc.* **155**, H661 (2008).

¹⁹L. Sygellou, S. Ladas, M. A. Reading, J. A. van den Berg, T. Conard, and S. De Gendt, *Surf. Interface Anal.* **42**, 1057 (2010).

²⁰P. Bailey (unpublished).

²¹E. H. Nicollian and J. R. Brews, *MOS Physics and Technology* (Wiley Interscience, New York, 1982).

²²E. Hourdakis, M. Theodoropoulou, A. G. Nassiopoulou, A. Parisini, M. A. Reading, J. A. van den Berg, T. Conard, and S. Degendt, *ECS Trans.* **25**, 363 (2009).

²³V. Gianneta, A. G. Nassiopoulou, C. A. Krontiras, and S. N. Georga, *Phys. Status Solidi C* **5**, 3686 (2008).

²⁴Y. Chung, J. C. Lee, and H. J. Shin, *Appl. Phys. Lett.* **86**, 022901 (2005).

²⁵A. Parisini, V. Morandi, S. Solmi, P. G. Merli, D. Giubertoni, M. Bersani, and J. A. van den Berg, *Appl. Phys. Lett.* **92**, 261907 (2008).

²⁶K. Kasahara, N. Uchitomi, T. Shimizu, K. Saki, and I. Mizushima, *Jpn. J. Appl. Phys.* **47**, 4461 (2008).